Vision-Based Relative State Estimation of Non-Cooperative Spacecraft Under Modeling Uncertainty

Shai Segal[1], Avishy Carmi[2], and Pini Gurfil[3]
Technion–Israel Institute of Technology, Haifa 32000, Israel

Abstract—Estimating the relative pose and motion of cooperative satellites using on-board sensors is a challenging problem. When the satellites are non-cooperative, the problem becomes far more complicated, as there might be poor or no *a priori* information about the motion or structure of the target satellite. In this work we develop robust algorithms for solving the said problem by assuming that only visual sensory information is available. Using two cameras mounted on a chaser satellite, the relative state of a target satellite, including the position, attitude, and rotational and translational velocities is estimated. Our approach employs a stereoscopic vision system for tracking a set of feature points on the target spacecraft. The perspective projection of these points on the two cameras constitutes the observation model of an EKF-based filtering scheme. In the final part of this work, the relative motion filtering algorithm is made robust to uncertainties in the inertia tensor. This is accomplished by endowing the plain EKF with a maximum a posteriori identification scheme for determining the most probable inertia tensor from several available hypotheses.

Table of Contents

1. Introduction

Estimating the relative state between space vehicles has attracted considerable research attention in the last decade [1]. Frequently, the relative state estimation problem is treated in the context of spacecraft formation flying [4] or rendezvous and docking [2], which are considered to be cooperative space missions. In these cases the relative sensing technique relies on information shared between the spacecraft. Normally, the relative sensor comprises of two separate devices such as two differential GPS receivers [3] or position-sensing diode (PSD) and light sources (beacons) [4] which are placed on the companion spacecraft at a known location.

Multiple spacecraft missions may involve interactions between non-cooperative vehicles such as tracking of resident space objects, on-orbit replenishment and responsive space missions [5]. When the satellites are non-cooperative, the problem of relative state estimation becomes far more complicated, as there might be poor or no *a priori* information about the motion or structure of the target satellite. Thus, the cooperative estimation architecture is inadequate.

Formation flying in the non-cooperative case can be realized by exploiting recent developments in the field of vision-based motion reconstruction. Resorting to vision-based estimation, benefits from the passive nature of visual sensing. In contrast to past methods, this setting does not require unique indicators (such as beacons) to be placed on the companion spacecraft. This renders the vision-based approach appealing for non-cooperative applications.

In vision-based systems, two-dimensional images of the three-dimensional scene acquired by a body-fixed camera usually lead to nonlinear implicit measurement equations. Moreover, due to the many-to-one mapping nature of the image projection, the magnitude of the translational velocity can be recovered only up to scale, yielding partial state estimation. In the current work, it is shown that the entire relative state (pose and motion) can be estimated using *two cameras* instead of a single one. By utilizing *stereoscopic* vision, depth information can be recovered and used for reconstructing the magnitude of the translational velocity vector in addition to its direction.

Stereo vision has been used in the past for estimating the relative state of two cooperative spacecrafts. The algorithm in Ref. [6], for example, utilizes a sequence of stereo images for determining the relative position and attitude of an orbiting satellite. Nevertheless, its capabilities in the non-cooperative settings are limited as it assumes that the feature point locations on the target are accurately modeled. In other cases where some *a priori* information about the target geometry is available, model matching techniques [7] can be used together with stereo vision.

978-1-4244-7351-9/11/$26.00 ©2011 IEEE
[1] Doctoral Student, Faculty of Aerospace Engineering. E-mail: shai@aerodyne.technion.ac.il
[2] Research Fellow, the Asher Space Research Institute, Technion, Haifa 32000, and senior lecturer, the Department of Mechanical Engineering, Ariel University Center, Ariel 47000. E-mail: ac599@cam.ac.uk
[3] Associate Professor, Faculty of Aerospace Engineering, Associate Fellow, AIAA. E-mail: pgurfil@technion.ac.il

There are few works in the literature that address the problem of relative state estimation of non-cooperative targets. In Refs.[8] and [9] the state and structure of an orbiting object are estimated using several cooperative satellites equipped with 3-D vision sensors (such as stereo cameras or laser-based). The main downfall of this method, however, is that it involves the acquisition of thousands of uniformly distributed data points for accurately tracking the rotating structure. The work of Ref. [10] considers an interesting approach in which stereo vision is used for autonomous rendezvous and robotic capturing of non-cooperative targets. Nonetheless, it lacks the practical implementation of its newly derived concepts.

As claimed in some of the above seminal works, the scaling factor ambiguity associated with stereo vision can be resolved assuming the baseline separating the two cameras is known. The feature points can then be accurately tracked by measuring their projections on the right and left stereo-rig planes. Moreover, the target attitude can be obtained by observing several points simultaneously [11].

Estimating the relative state directly from the visual measurements involves the formulation of highly nonlinear observation and process models. These normally consist of additional uncertainties associated with non-cooperative targets. The main purpose of this work, therefore, is to design a robust filtering scheme for handling the additional complications encountered in such scenarios. The estimation scheme proposed inhere consists of multiple iterated extended Kalman filters (IEKFs) and a maximum a posteriori (MAP) inertia tensor identification algorithm. It should be noted that this approach is somewhat similar to the acclaimed multiple model KF technique [12], which is vastly used for filtering under modeling uncertainties. The key idea underlying this architecture can be summarized as follows. It is typically easier to propagate a conditional probability density function (pdf) than its associated joint pdf. In our case, each individual IEKF approximates the pdf of the relative state (given the observation history) conditioned on the inertia tensor. This in turn facilitates the application of a Bayesian MAP estimator for recognizing the most probable inertia hypothesis based on the obtained conditional. The decisive advantage of using this approach is demonstrated via an extensive numerical study.

In addition to the above, we also demonstrate the performance gain (in terms of estimation accuracy) when using a recently introduced dynamical model taking into account the kinematic coupling between the rotational and translational motions [13].

2. Mathematical Formulation

Suppose that two rigid-body spacecraft are in orbit around the Earth. It is assumed that the chaser spacecraft, denoted here by C, is equipped with vision sensors used for acquiring images of a set of N feature points located on a target spacecraft, T. These feature points can be represented as N vectors, $\{\mathbf{P}_i\}_{i=1}^{N}$, in some reference frame.

Reference Frames and Notations

The reference frames and notations used in the ensuing are similar to those in Ref. [13] and are revised here for completeness. $\mathscr{L}$ – a local-vertical, local-horizontal (LVLH) Euler-Hill reference frame fixed to the chaser spacecraft center-of-mass (CM), with $\hat{\mathbf{x}}$ being a unit vector directed from the spacecraft radially outward, $\hat{\mathbf{z}}$ normal to the chaser orbital plane, and $\hat{\mathbf{y}}$ completes the triad; $\mathcal{L}$ – a Cartesian right-hand body-fixed reference frame attached to the chaser spacecraft CM; and $\mathcal{T}$ – a Cartesian right-hand body-fixed reference frame attached to the target spacecraft CM. In what follows we assume that the orbital frame $\mathscr{L}$ is aligned with the body-fixed frame, $\mathcal{L}$

Let $\mathbf{P}_{i|\mathcal{T}} \in \mathbb{R}^3$ be an arbitrary feature vector directed from the origin of the coordinate system $\mathcal{T}$ to some feature point $P_{i|\mathcal{T}}$ on the target spacecraft. For notational simplicity, we will omit the subscript $|_{\mathcal{T}}$ from that point onwards.

The vector $\boldsymbol{\rho}_i = [\rho_i^1, \rho_i^2, \rho_i^3]^T \in \mathbb{R}^3$ denotes the position of P_i relative to the CM of C, resolved in frame $\mathcal{L}$, and $\dot{\boldsymbol{\rho}}_i = [\dot{\rho}_i^1, \dot{\rho}_i^2, \dot{\rho}_i^3]^T$ denotes the corresponding components of the relative translational velocities resolved in $\mathcal{L}$. A feature point that is located on the CM of T would be denoted by P_0 where its corresponding relative position and velocity vectors would be denoted by $\boldsymbol{\rho}_0$ and $\dot{\boldsymbol{\rho}}_0$, respectively.

In addition, we denote $\boldsymbol{\omega} \in \mathbb{R}^3$ the angular velocity of T relative to C resolved in $\mathscr{L}$. The attitude of T relative to C is parameterized using the rotation quaternion (defined on the 3-sphere) $\mathbf{q} = [\boldsymbol{\varrho}^T, q_4]^T \in \mathbb{S}^3$ where $\boldsymbol{\varrho}$ and q_4 denote its vector and scalar parts, respectively. The attitude matrix associated with $\mathbf{q}$, denoted as $D(\mathbf{q})$, is given by

$$D(\mathbf{q}) = [(q_4)^2 - \boldsymbol{\varrho}^T\boldsymbol{\varrho}]I_{3\times 3} + 2\boldsymbol{\varrho}\boldsymbol{\varrho}^T - 2q_4[\boldsymbol{\varrho}\times]$$

where $[\mathbf{v}\times]$ is the cross-product matrix (that is, the matrix satisfying $[\mathbf{v}\times]\mathbf{u} = \mathbf{v}\times\mathbf{u}$).

Problem Statement

Our objective can be summarized as follows. We are interested in estimating the relative state

$$\mathbf{x} = [\boldsymbol{\rho}_0^T,\ \dot{\boldsymbol{\rho}}_0^T,\ \boldsymbol{\omega}^T,\ \mathbf{q}^T]^T \in \mathbb{R}^{13}$$

as well as the structure of T, which is represented by a set of feature points and possibly other unknown parameters (e.g. inertia tensor, external torques), using a sequence of stereo images.

3. Bayesian Filtering Approach

Formally, we treat $\mathbf{x}$ as a stochastic process for which the dynamics is described by (following the common white noise engineering notation)

$$\dot{\mathbf{x}} = f(\mathbf{x}) + \xi \tag{1}$$

where ξ is zero mean white noise with power spectral density matrix Q. The explicit form of the nonlinear function $f(\mathbf{x})$

is deferred to the appendix for improved reading. The initial distribution of $\mathbf{x}$ is specified by $p(\mathbf{x}_0)$. In what follows we augment the state vector $\mathbf{x}$ with the feature point locations for handling the uncertainties associated with the target structure, that is,

$$\mathbf{x} = [\boldsymbol{\rho}_0^T,\ \dot{\boldsymbol{\rho}}_0^T,\ \boldsymbol{\omega}^T,\ \mathbf{q}^T, \mathbf{P}_1^T, \ldots, \mathbf{P}_N^T]^T \in \mathbb{R}^{13+3N}$$

. In the Bayesian framework we associate each such point with a prior $p(\mathbf{P}_i)$ that reflects our knowledge of its location. As these points are typically fixed in the target reference frame, they may be regarded as random parameters.

Normally, a likelihood function relates the observation to the unknown states. In our case this function relies on the perspective projection model [14],[15],[16] (a brief overview of this model is provided in the Appendix). The underlying observation model which constitutes the likelihood is described below.

Observation Model

A stereo rig system is composed of two cameras where, in our case, the right camera is the primary one and its center of projection coincides with the CM of C. The two cameras are separated by a base line b along the X axis (see Fig. 1). Following this, the relative position, $\boldsymbol{\rho}_i$, between the right (primary) camera center of projection and the observed feature point, $\mathbf{P}_i$, satisfy

$$\boldsymbol{\rho}_i = \boldsymbol{\rho}_0 + D(\mathbf{q})\mathbf{P}_i \tag{2}$$

The observations acquired by the primary camera are merely the perspective projection $\pi : \mathbb{R}^3 \rightarrow \mathbb{R}^2$ of these feature points onto the image plane, that is

$$\pi(\boldsymbol{\rho}_i) = \begin{bmatrix} \rho_i^1/\rho_i^2 \\ \rho_i^3/\rho_i^2 \end{bmatrix} \tag{3}$$

As both cameras are separated by a fixed baseline $\mathbf{b} = [b, 0, 0]^T$, we may write down the observations corresponding to the ith feature point as

$$\boldsymbol{\epsilon}_i^r \triangleq \pi(\boldsymbol{\rho}_i),\ \boldsymbol{\epsilon}_i^l \triangleq \pi(\boldsymbol{\rho}_i + \mathbf{b}^T)$$

(See Fig. 1). Further letting

$$\mathbf{z_i} \triangleq \begin{bmatrix} \boldsymbol{\epsilon}_i^r \\ \boldsymbol{\epsilon}_i^l \end{bmatrix},\ \ h_i(\mathbf{x}) \triangleq [\pi(\boldsymbol{\rho}_i)^T,\ \pi(\boldsymbol{\rho}_i + \mathbf{b})^T]^T \tag{4}$$

the observation model can be rewritten in a compact fashion as

$$\mathbf{z_i}_k = h_i(\mathbf{x}_k) + n_{ik},\ \ i = 1, \ldots, N \tag{5}$$

where n_{ik} denotes a zero-mean white noise process with covariance R. Following this, it can be readily recognized that the overall dimension of the observation vector $[\mathbf{z_1}_k^T, \mathbf{z_2}_k^T, \ldots, \mathbf{z_N}_k^T]^T$ is $4N$.

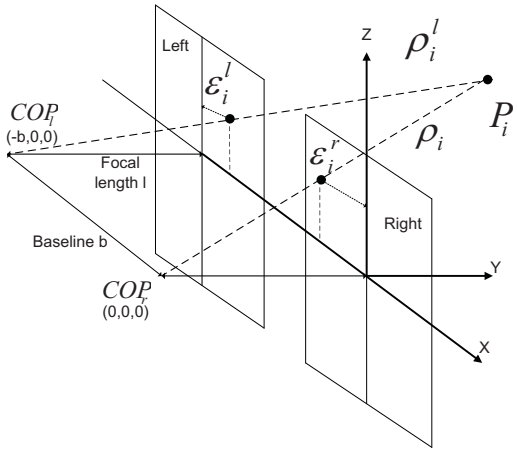

Figure 1. The stereo-rig system. The right camera's center-of-projection coincides with the origin of the target body frame $\mathcal{C}$.

Incorporating Kinematic Couplings in the Process Model

The rigid body motion comprises of both translational and rotational components. In other words, these two distinct types of movement are coupled [13]. As this is an intrinsic property of the underlying system, one should carefully assess the propriety of any simplified model lacking such a coupling. In this work we have compared the performance of our filtering scheme when using either modeling approaches: the commonly employed simplified (uncoupled) model, and a recently introduced model that accounts for this kinematic coupling [13] (for convenient, this model is provided in the Appendix).

The advantage of the coupling approach over the commonly used one has been already demonstrated in a recent work [17]. Our results, which are summarized in the numerical study section of this work, have shown a similar trend. Specifically, an improved accuracy has been attained in estimating the relative position components. Nevertheless, it should be noted that adopting this approach essentially involves the inclusion of additional states accounting for the relative positions of individual feature points.

4. ESTIMATION METHODOLOGY

The optimal (in the mean square error sense) estimator is implicitly given by

$$\hat{\mathbf{x}}_k = E\left\{\mathbf{x}_k \mid z_{1:k}\right\}$$

where the expectation is taken with respect to the filtering pdf, that is the conditional pdf of x_k given the observation history $z_{1:k} = \{\mathbf{z}_1, \ldots, \mathbf{z}_k\}$. A sequential scheme for propagating this pdf is provided by the acclaimed Bayesian recursion [18]. Nonetheless, this recursion is, in general, analytically intractable in the nonlinear non-Gaussian case. There are a few known methods for approximating the statistics of the filtering pdf such as sequential Monte Carlo, Grid-based approaches, and the nonlinear KF variants, the UKF and EKF [18]. Unfortunately, the high dimensionality of the problem at hand renders most of the previously mentioned state-of-the-art nonlinear filtering methods strictly inadequate. As was previously mentioned, the estimation scheme adopted inhere relies on the iterated EKF [**?**]. Before we proceed in describing the proposed filtering scheme, however, we would like to discuss the following crucial issue.

Coping with Inertia Uncertainties

A major consideration in this work is given to the modeling uncertainty associated with the target spacecraft inertia tensor. In the attitude determination community this problem was addressed in the past, especially within the framework of angular-rate filtering. It has been shown that such uncertainty considerably affects the numerical stability of angular-rate estimation schemes owing to the sensitivity of the Euler equation [19],[20],[21]. In this work we alleviate this caveat following an approach that is somewhat related to the one suggested in Refs.[20],[21] where an external estimator is interlaced with the main filtering algorithm. In particular, we develop an inertia identification scheme that involves the evaluation of a likelihood score over a finite set of possibilities $\mathcal{I} = \{I_i\}_{i=1}^{N_I}$. As it is shown in the ensuing, this procedure relies on the innovations process of the IEKF assuming the actual inertia is one of the hypotheses. The resulting scheme consists of several IEKF's working in parallel, each is aimed at approximating

$$\hat{\mathbf{x}}_k(I_i) = E\left\{\mathbf{x}_k \mid z_{1:k}, I_i\right\}$$

Robust Relative State Filtering via Multi IEKF

Our filtering scheme consists of several IEKF's working simultaneously. Each filer employs the previously described observation and process models and assumes an hypothetical target inertia tensor I_i. The obtained statistics from the filters are then used for identifying the most probable inertia hypothesis. The detailed identification procedure is described next.

In what follows we assume that the inertia tensor is a random parameter with some known prior pdf $p(I)$. Recalling Bayes rule we may write

$$p(I \mid z_{1:T}) \propto p(z_{1:T} \mid I)p(I) \tag{6}$$

where $p(z_{1:T} \mid I)$ is the likelihood of the observation history conditioned on the inertia tensor. It can be readily recognized that the likelihood can be written as

$$p(z_{1:T} \mid I) = \prod_{k=1}^{T} p(z_k \mid I, z_{1:k-1}) \tag{7}$$

where it was implicitly assumed that $p(z_1 \mid I, z_{1:0}) \triangleq p(z_1 \mid I)$. Further elaborating the right hand side term in (7) yields

$$\begin{aligned} &p(z_k \mid I, z_{1:k-1}) = \\ &\int\int p(z_k \mid \mathbf{X}_k)p(\mathbf{X}_k \mid \mathbf{X}_{k-1}, I)p(\mathbf{X}_{k-1} \mid z_{1:k-1})d\mathbf{X}_k d\mathbf{X}_{k-1} \\ &= \int p(z_k \mid \mathbf{X}_k)p(\mathbf{X}_k \mid z_{1:k-1}, I)d\mathbf{X}_k \\ &= E\left\{p(z_k \mid \mathbf{x}_k) \mid z_{1:k-1}, I\right\} \end{aligned} \tag{8}$$

Assuming the conditional covariance $\mathrm{cov}\left(\mathbf{x}_k \mid z_{1:k-1}, I\right)$ is sufficiently small, the above expectation can be approximated by

$$E\left\{p(z_k \mid \mathbf{x}_k) \mid z_{1:k-1}, I\right\} \approx p(z_k \mid \hat{\mathbf{x}}_k^+(I)) \tag{9}$$

where

$$\hat{\mathbf{x}}_k^+(I) = E\{\mathbf{x}_k \mid z_{1:k-1}, I\} \tag{10}$$

is the propagated conditional mean. In our settings, $\hat{\mathbf{x}}_k^+(I_i)$ is estimated by an individual IEKF with a hypothetical inertia tensor $I = I_i$. Further assuming that the observation noise is Gaussian yields

$$p(z_k \mid \hat{\mathbf{x}}_k^+(I)) = c \cdot \exp\left\{-\frac{1}{2} \parallel \mathbf{z}_k - h(\hat{\mathbf{x}}_k^+(I)) \parallel_{R^{-1}}^2\right\} \tag{11}$$

where $\parallel \mathbf{a} \parallel_P^2 \triangleq \mathbf{a}^T P \mathbf{a}$. Finally, (7) – (11) implies

$$\log p(z_{1:T} \mid I) \approx T \log c - \frac{1}{2}\sum_{i=1}^{T} \parallel \mathbf{z}_i - h(\hat{\mathbf{x}_i}^+(I)) \parallel_{R^{-1}}^2 \tag{12}$$

which essentially consists of computing the innovations of each filter over the time interval $[1, T]$. The most probable inertia hypothesis can be then obtained via solving

$$\hat{I} = \arg\max_{I \in \mathcal{I}} \log p(z_{1:T} \mid I) + \log p(I) \tag{13}$$

5. NUMERICAL STUDY

An extensive Monte-Carlo simulation study has been conducted for assessing the performance of the derived filtering scheme. The following example consists of two low earth orbiting (LEO) satellites. The chaser satellite orbital parameters are set as $e_C = 0.05$ and $a_C = 7170$ km. In all runs, the chaser inertia tensor is assumed to be diagonal,

$I_C = \text{diag}(100, 120, 130)\ \text{kg}\,\text{m}^2$. The target inertia, on the other hand, is set as

$$I_T = \begin{bmatrix} 96 & 43 & 26 \\ 43 & 104 & 10 \\ 20 & 10 & 133 \end{bmatrix} \tag{14}$$

The chaser satellite is equipped with a stereo vision system consisting of two cameras with a baseline of $b = 1\,\text{m}$. In this example it is assumed that there are exactly 10 feature points of which the locations are uniformly spread over the target surface, that is

$$\{P_{x_i},\, P_{y_i},\, P_{z_i}\}|_{\mathcal{F}} \sim \mathcal{U}(-1.5\ \text{m},\ 1.5\ \text{m}), \quad \forall i \tag{15}$$

The observation noise is assumed to be zero-mean Gaussian with a standard deviation of 10^{-5}. The relative state initial conditions are set as

$$\boldsymbol{\rho}_0(0) = [10, 100, 10]^T\,\text{m} \tag{16a}$$

$$\dot{\boldsymbol{\rho}}_0(0) = [0.01, -0.0225, -0.01]^T\,\text{m}\,/\,\text{s} \tag{16b}$$

$$\boldsymbol{\omega}_C(0) = [0, 0, \dot{f}_L(0)]^T\,\text{rad} \tag{16c}$$

$$\boldsymbol{\omega}_T(0) = [0.1, 0.1, 0.1]^T\,\text{deg}\,/\,\text{s} \tag{16d}$$

$$\boldsymbol{\omega}(0) = D(0)\boldsymbol{\omega}_T(0) - \boldsymbol{\omega}_C(0) \tag{16e}$$

where $\dot{f}_C(0) = 0.0656\ \text{deg}\,/\,\text{s}$ (see Appendix for the detailed model parameters). The initial relative attitude is set as $\mathbf{q} = [0, 0, 0, 1]^T$ in all runs.

The robust multiple IEKF scheme uses 5 hypotheses of the target inertia tensor. These hypotheses are randomly sampled from a Wishart distribution in the following manner

$$I_i = I_T + \delta I_i, \quad \delta I_i \sim \mathcal{W}(\sigma_{I_T}, DF), \quad i = 1, \ldots, 5 \tag{17}$$

with $\sigma_{I_T} = \frac{1}{3} I_T I_T^T$ and $DF = 3$. In what follows the robust multiple IEKF scheme is compared with a single IEKF that uses a randomly chosen inertia tensor (from the set of hypotheses).

Results

The performance (based on 100 MC runs) of the plain IEKF algorithm that is aware of the true target inertia is depicted in Figs (2(a)) – (3), whereas the performance (based on 1000 MC runs) of the robust multi IEKF scheme is shown in Figs. (4(b)) – (4(a)). Figures (2(a)) – (2(d)) depict the distribution of the norm estimation errors of the relative states via the 50, 70 and 90 percentile lines. The distribution of the norm estimation errors of the feature points is shown in Fig. (3). The distribution of the relative attitude errors of the plain and robust filtering schemes are shown in Fig. (4(a)) and (4(b)), respectively. Finally, the effect of incorporating the kinematic coupling of the translational and rotational components is demonstrated in the remaining figures (5(a)) – (6).

The results clearly demonstrate the feasibility of vision-based relative state estimation under modeling uncertainty. The benefit of using the robust multiple IEKF filtering scheme is illustrated by its improved attitude estimation accuracy.

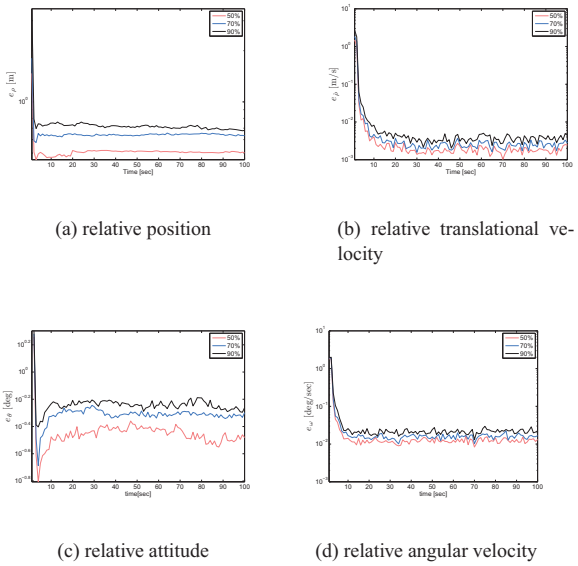

(a) relative position

(b) relative translational velocity

(c) relative attitude

(d) relative angular velocity

Figure 2. The distribution of the norm estimation errors (shown via the 50, 70 and 90 percentiles) of the relative position 2(a), translational velocity 2(b), relative attitude 2(c), and angular velocity 2(d).

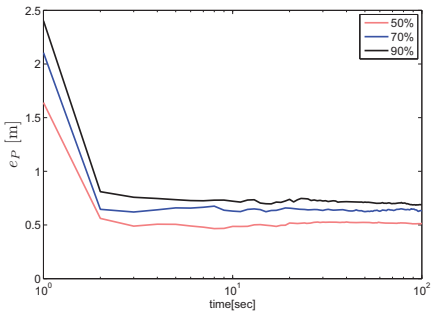

Figure 3. The distribution of the norm estimation errors (shown via the 50, 70 and 90 percentiles) of the feature points.

6. CONCLUSIONS

This paper develops a stereo-vision based filtering algorithm for estimating the relative state of two non-cooperative spacecraft. The proposed scheme employs multiple IEKF's each with a different hypothetical target inertia. This architecture is shown to significantly improve the robustness of the algorithm to inertia modeling uncertainties. In addition to that, our work corroborates the benefits of incorporating kinematic coupling between the translational and rotational dynamics.

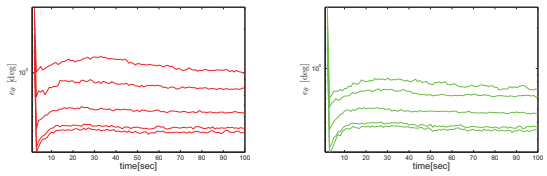

(a) plain IEKF (b) robust multiple IEKF

Figure 4. The distribution of the relative attitude estimation errors (shown via the 45, 50, 70, 90 and 95 percentiles) of the robust multiple IEKF filtering scheme 4(b), and of the plain IEKF with a randomly chosen target inertia 4(a).

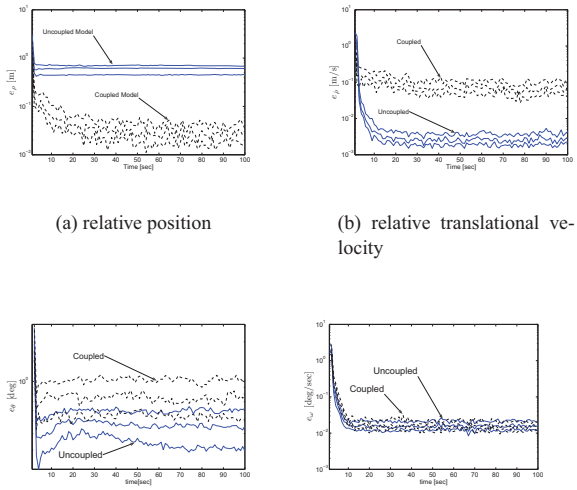

(a) relative position (b) relative translational velocity

(c) relative attitude (d) relative angular velocity

Figure 5. Effect of kinematic coupling. The distribution of the norm estimation errors (shown via the 50, 70 and 90 percentiles) of the relative position 5(a), translational velocity 5(b), relative attitude 5(c), and angular velocity 5(d).

APPENDICES

A. RELATIVE SPACECRAFT DYNAMICS

The transitional relative dynamics between the CMs of T and C, resolved in $\mathscr{L}$, can be written as (see Ref.[13])

$$\begin{aligned}
\ddot{\rho}_0^1 &= 2\dot{\nu}_C\dot{\rho}_0^2 + \ddot{\nu}_C\rho_0^2 + \dot{\nu}_C^2\rho_0^1 - \frac{\mu(r_C+\rho_0^1)}{r_T^3} + \frac{\mu}{r_C^2} \\
\ddot{\rho}_0^2 &= 2\dot{\nu}_C\dot{\rho}_0^1 - \ddot{\nu}_C\rho_0^1 + \dot{\nu}_C^2\rho_0^2 - \frac{\mu\rho_0^2}{r_T^3} \\
\ddot{\rho}_0^3 &= -\frac{\mu\rho_0^3}{r_T^3}
\end{aligned} \tag{18}$$

where $r_T \triangleq [(r_C+\rho_0^1)^2 + {\rho_0^2}^2 + {\rho_0^3}^2]^{0.5}$ and ν_C is the chaser true anomaly, and r_C is the chaser CM position in inertial frame (see Ref. [13]).

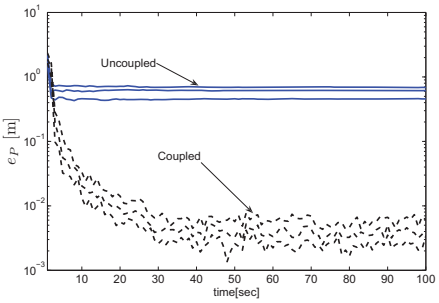

Figure 6. Effect of kinematic coupling. The distribution of the norm estimation errors (shown via the 50, 70 and 90 percentiles) of the feature points.

The relative rotational dynamics are written for both spacecraft using their respective inertia tensors $I_C,\ I_T \in \mathbb{R}^{\text{⊮}\times\text{⊮}}$, and external torques, $\mathbf{N}_C,\ \mathbf{N}_T \in \mathbb{R}^{\text{⊮}}$, that is

$$\begin{aligned}
I_C\dot{\boldsymbol{\omega}} = {} & I_C D(\mathbf{q}) I_T^{-1} \\
& \left[\mathbf{N}_T - D^T(\mathbf{q})(\boldsymbol{\omega}+\boldsymbol{\omega}_C)\times I_T D^T(\mathbf{q})(\boldsymbol{\omega}+\boldsymbol{\omega}_C)\right] \\
& - I_C\boldsymbol{\omega}_C\times\boldsymbol{\omega} - \left[\mathbf{N}_C - \boldsymbol{\omega}_C\times I_C\boldsymbol{\omega}_C\right]
\end{aligned} \tag{19}$$

where the relative attitude kinematics is given by[13]

$$\dot{\mathbf{q}} = \frac{1}{2}Q(\mathbf{q})\boldsymbol{\omega}|_{\mathcal{T}} \tag{20}$$

with $\boldsymbol{\omega}|_{\mathcal{T}} = D^T(\mathbf{q})\boldsymbol{\omega}|_{\mathcal{L}} = \boldsymbol{\omega}_T - D^T(\mathbf{q})\boldsymbol{\omega}_C$ and

$$Q(\mathbf{q}) = \begin{bmatrix} q_4 I_{3\times 3} + [\boldsymbol{\varrho}\times] \\ -\varrho^T \end{bmatrix} \tag{21}$$

The complete translational-rotational model is

$$\dot{\mathbf{x}} = \mathbf{f}(\mathbf{x}) + \xi \tag{22}$$

where $f : \mathbb{R}^{13} \to \mathbb{R}^{13}$ is given by

$$f(\mathbf{x}) = [f_{\rho_0}(\mathbf{x}),\ f_{\dot{\rho}_0}(\mathbf{x}),\ \ f_\omega(\mathbf{x}),\ f_q(\mathbf{x})] \tag{23}$$

and

$$f_{\rho_0}(\mathbf{x}) = \dot{\boldsymbol{\rho}}_0,\ \ f_{\dot{\rho}_0}(f) = \ddot{\boldsymbol{\rho}}_0,\ \ f_\omega(\mathbf{x}) = \dot{\omega},\ \ f_q(\mathbf{x}) = \dot{q} \tag{24}$$

Note that this model is rather a simplified one, as the rotational and translational components are essentially uncoupled. A kinematic coupling can be incorporated upon recalling [13]

$$\ddot{\boldsymbol{\rho}}_i = \ddot{\boldsymbol{\rho}}_0 + \dot{\boldsymbol{\omega}}\times\boldsymbol{\rho}_i + \boldsymbol{\omega}\times(\boldsymbol{\omega}\times\boldsymbol{\rho}_i) \tag{25}$$

B. Stereo Rig and Perspective Projection

Suppose that a stereo rig is mounted rigidly on C and is pointed at T. The stereo rig is composed of two parallel cameras wherein the right camera's center-of-projection, COP_r, is located on the CM of C, and the left camera's center-of-projection, COP_l, is separated by a baseline distance b from COP_r. Then the corresponding COP vectors are (See Fig. 1)

$$\mathbf{COP}_r \equiv \mathbf{P}_C^0 = [0,0,0]^T and, \mathbf{COP}_l = [-b,0,0]^T \quad (26)$$

For the right camera we define a frame, $\mathcal{C}$, which is a 3D Cartesian right-hand coordinate system originating at COP_r. The fundamental plane is perpendicular to the right camera's image plane. The unit vector $\hat{\mathbf{x}}$ is horizontal, pointing from COP_l to COP_r; $\hat{\mathbf{z}}$ is vertical, positive upwards; and $\hat{\mathbf{y}}$ completes the right-hand setup. For simplicity, it is assumed that this frame's axes are aligned with the axes of $\mathcal{C}$. The reference frame $\mathcal{M}$ is a two-dimensional coordinate system, contained in the image plane, and is parallel to the $\hat{\mathbf{x}}$ and $\hat{\mathbf{z}}$ axes of the $\mathcal{C}$ system, at a distance l from COP_r away from the observed object. The distance l is the focal length.

When a feature point on T, $\{P_i\}_{i=1}^N$, is viewed by the stereo rig, the perspective projection model $\pi : \mathbb{R}^3 \rightarrow \mathbb{R}^2$ is used to describe its corresponding visual observations. This model projects the a 3D coordinate of a point onto a 2D image plane.

References

[1] Alfriend, K. T., Vadali, S. R., Gurfil, P., How, J. P., and Breger, L. S., *Spacecraft Formation Flying: Dynamics, Control and Navigation*, Elsevier, Oxford, 2009; Chapter 1, pp. 1–8.

[2] Philip, N. K. and Ananthasayanam, M. R., "Relative Position and Attitude Estimation and Control Schemes for the Final Phase of an Autonomous Docking Mission of Spcecraft," *Acta Astronautica*, Vol. 52, 2003, pp. 511–522.

[3] Robertson, A., Corazzini, T., and How, J. P., "Formation Sensing and Control Technologies for a Separated Spacecraft Interferometer," *Proceedings of the American Control Conference*, Philadelphia, Pennsylvania, June. 1998, pp. 1574–1579.

[4] Kim, S. G., Crassidis, J. L., Cheng, Y., and Fosbury, A. M., "Kalman Filtering for Relative Spacecraft Attitude and Position Estimation," *Jouranl of Guidance, Control, and Dynamics*, Vol. 30, No. 1, January-February 2007, pp. 133–143.

[5] Jumper, J. P., "Counterspace Operations," Tech. Rep. 2-2.1, United State Air Force, 2 August 2004.

[6] Giancarmine, F., Michele, G., and Domenico, A., "A Stereo-Vision Based System for Autonomous Navigation of an In-Orbit Servicing Platform," *Proceedings of AIAA Infotech@Aerspace Conference*, AIAA, Seattle, Washington, April 2009, Paper No. AIAA-2009-1934.

[7] Fuyuto, T., Heihachiro, K., and N., S. I., "Motion Estimation to a Failed Satellite on Orbit using Stereo Vision and 3D Model Matching," *International Conference on Control, Automation, Robotics and Vision ICARCV*, IEEE, 2006.

[8] Lichter, D. M. and Dubowsky, S., "State,Shape and Parameter Estimation of Space Objects from Range Images," *Proceedings of the 2004 IEEE International Conference on Robotics and Automation*, New Orleans, LA, April 2004.

[9] Lichter, D. M. and Dubowsky, S., "Estimation of state, shape and inertial parameter of space objects from sequences of range images," *Proceedings of the SPIE Conference on Intelligent Robotics and Computer Vision*, Providence, RI, Oct. 2003.

[10] Xu, W., Liang, B., Li, C., and Xu, Y., "Autonomous rendezvous and robotic capturing of non-cooperative target in space," *Robotica*, Vol. 28, 2010, pp. 705–718.

[11] Ullman, S., *The Interpretation of Visual Motion*, The MIT Press Series in Artificial Intelligence, 1979; Chapter 4, pp. 146.

[12] Bar-Shalom, Y., X., R. L., and Kirubarajan, T., *Estimation with Application to Tracking and Nacigation*, John wiley and soms, inc, 2001; Chapter 11, pp. 441–481.

[13] Segal, S. and Gurfil, P., "Effect of Kinematic Rotation-Translation Coupling on Relative Spacecraft Translational Dynamics," *Journal of Guidance, Control and Dynamics*, Vol. 32, No. 3, May-June 2009, pp. 1045–1050.

[14] Soatto, S., Frezza, R., and Perona, P., "Motion Estimation via Dynamic Vision," *IEEE Transactions on Automatic Control*, Vol. 41, No. 3, March 1996, pp. 393–413.

[15] Soatto, S. and Perona, P., "Recursive 3-D Visual Motion Estimation Using Subspace Constraints," *International Journal of Computer Vision*, Vol. 22, No. 3, 1997, pp. 235–259.

[16] Gurfil, P. and Rotstein, H., "Partial Aircraft State Estimation from Visual Motion Using the Subspace Constraints Approach," *Journal of Guidance, Control and Dynamics*, Vol. 24, No. 5, Sep.-Oct. 2001, pp. 1016–1028.

[17] Y., X., "Relative position and attitude estimation for satellite formation with coupled translational and rotational dynamics," Vol. 104, February 2000, pp. 139–158, Also Paper AAS 00-012 of the AAS Guidance and Control Conference.

[18] Ristic, B., Arulampalam, S., and Gordon, N., *Beyond the Kalman Filter*, Artech House, 2004.

[19] Psiaki, M. L. and Oshman, Y., "Spacecraft Attitude Rate Estimation From Geomagnetic Field Measurements,,"

Journal of Guidance, Control and Dynamics, Vol. 26, No. 2, March-April 2003, pp. 244–252.

[20] Tortora, P., O. Y. and Santoni, F., "Spacecraft Angular Rate Estimation from Magnetometer Data Only Using an Analytic Solution of Eulers Equations," *Journal of Guidance, Control and Dynamics*, Vol. 27, No. 3, 2004, pp. 365–373.

[21] Carmi, A. and Oshman, Y., "Robust Spacecraft Angular Rate Estimation from Vector Observations Using Interlaced Particle Filtering," *Journal of Guidance, Control and Dynamics*, Vol. 30, No. 6, November–December 2007, pp. 1729–1741.